Microsc. Microanal. 22, 1360–1368, 2016
doi:10.1017/S1431927616011788

Microscopy AND Microanalysis

Determination of the Effective Detector Area of an Energy-Dispersive X-Ray Spectrometer at the Scanning Electron Microscope Using Experimental and Theoretical X-Ray Emission Yields

Mathias Procop,[1,†] Vasile-Dan Hodoroaba,[1,*] Ralf Terborg,[2] and Dirk Berger[3]

[1]*Division 6.1 Surface Analysis and Interfacial Chemistry, Federal Institute for Materials Research and Testing (BAM), 12200 Berlin, Germany*
[2]*Bruker Nano GmbH, 12489 Berlin, Germany*
[3]*Center for Electron Microscopy (ZELMI), Technical University of Berlin, 10623 Berlin, Germany*

Abstract: A method is proposed to determine the effective detector area for energy-dispersive X-ray spectrometers (EDS). Nowadays, detectors are available for a wide range of nominal areas ranging from 10 up to 150 mm^2. However, it remains in most cases unknown whether this nominal area coincides with the "net active sensor area" that should be given according to the related standard ISO 15632, or with any other area of the detector device. Moreover, the specific geometry of EDS installation may further reduce a given detector area. The proposed method can be applied to most scanning electron microscope/EDS configurations. The basic idea consists in a comparison of the measured count rate with the count rate resulting from known X-ray yields of copper, titanium, or silicon. The method was successfully tested on three detectors with known effective area and applied further to seven spectrometers from different manufacturers. In most cases the method gave an effective area smaller than the area given in the detector description.

Key words: energy-dispersive X-ray spectrometer (EDS), EDX, effective area, X-ray emission yield, geometrical collection efficiency

Introduction

Soon after the publication by Kemmer et al. (1987) on application of the silicon drift detector (SDD) principle as a detector for X-ray spectroscopy, this detector type experienced an amazing development. In 1997, it gained its first commercial application in the form of a compact instrument for X-ray fluorescence analysis provided by Röntec GmbH (Berlin, Germany); and the same company brought the first spectrometer equipped with SDD as an attachment for the scanning electron microscope (SEM) onto the market in 2000 as "XFlash®." The only manufacturer of the SDD chip at that time was the German company Ketek (Ketek, 2016). One of the authors (M.P.) had the opportunity to perform experiments with the XFlash® of the first series. It was only a spectrometer with a 5 mm^2 detector area, at that time with a beryllium window and an energy resolution of about 180 eV for Mn-Kα, but already able to handle an input count rate of one million cps. The first high qualitative X-ray maps with 512 × 384 pixels and collected in 1 min were published by Procop et al. (2002).

Of course, a spectrometer's ability to handle extremely high count rates can be exploited only in the case of specimens with a large X-ray yield (photons/electron/sr), and able to endure high probe currents (above 10 nA) without damage. In order to also have high count rates at low probe currents and X-ray yields, manufacturers improved not only light element performance and energy resolution of energy-dispersive X-ray spectrometers (EDS) with SDD, but also increased the detector area. Currently, the SDD with the largest area is the 150 mm^2 X-Max, introduced by Oxford Analytical Instruments in 2013 (Oxford Instruments, 2016). However, the measured count rate is not only a function of detector area, but it depends on the solid angle of detection defined by the particular geometry of the EDS in the SEM chamber. A large area detector positioned at large distance from the specimen will collect a similar number of photons/s/nA as a smaller detector closer to the specimen. This was discussed in recent publications by Zaluzec (2009*a*, 2009*b*, 2014).

The solid angle of detection can be determined experimentally by the aperture method: apertures of known size are placed in front of the detector and their distance to the specimen must be measured, usually by a ruler. After collecting spectra from any specimen at constant probe current and live time, the extrapolation of peak intensity versus aperture area toward the measured intensity without aperture gives the solid angle of detection. This method has been applied by several authors when X-ray yields were measured, e.g. Lifshin et al. (1980); Maenhaut & Raemdonck (1984); Procop (2004).

As mentioned, the knowledge of the solid angle of detection does not give an answer concerning the detector area. For a spectrometer specified according to the related

Received April 28, 2016; accepted September 20, 2016
*Corresponding author. Dan.Hodoroaba@bam.de
† Current address: IfG-Institute for Scientific Instruments, 12489 Berlin, Germany.

ISO standard 15632 (ISO 15632, 2012), the user will find in most cases one or more of the following specifications: (a) a general description of the spectrometer including the net active sensor area to evaluate its performance, (b) the energy resolution with corresponding input count rate and dead time, (c) the P/B ratio in the Fe^{55} spectrum, and finally, (d) the L/K intensity ratio in a Ni or Cu spectrum to estimate spectrometer efficiency at low energies. Items (b)–(d) can be checked by the user. Related procedures are recommended in the annexes of the standard, however, the "net active sensor area (after collimation)" is missing in most cases. Aside from a few exceptions, it is not mentioned whether a given detector area means the chip size or the net active sensor area. Because the net active area may be reduced by an additional collimator, an electron trap in front of the detector and shadowing by other parts in the SEM chamber, we define as effective area that detector area illuminated by X-rays under the condition of the specific installation.

The question arises whether it is possible to determine the effective detector area by a simple experiment, which can be performed by the SEM/EDS operator herself/himself. The answer is yes. Only two preconditions must be given: (1) the SEM must allow accurate probe current measurement, either by an internal or by an external amperemeter, and (2) the detector must be retractable, and the vector of motion has to be directed to the X-ray source point on specimen in the analytical working distance. Both preconditions are fulfilled for most SEM/EDS configurations.

Materials and Methods

According to Castaing & Descamps (1955), the number of photons per primary electron per steradian, *emitted* in the direction of the take-off angle θ can be written as

$$\frac{N(\theta)}{4\pi} = f(\chi)\frac{N}{4\pi}, \tag{1}$$

where $N/4\pi$ is the number of *generated* photons per steradian per electron and $f(\chi)$ means the absorption correction term. The net count rate I of a characteristic X-ray line, measured with a spectrometer having the efficiency ε at the energy of the line and collecting the radiation emitted into the solid angle Ω is then

$$I = \Omega\epsilon\frac{i_p}{e}\frac{N(\theta)}{4\pi}, \tag{2}$$

with i_p meaning the probe current in Ampere and e the electron charge in Coulomb. Differentiating equation (2) we have

$$\frac{dI}{d\Omega} = \epsilon\frac{i_p}{e}\frac{N(\theta)}{4\pi}.$$

Therefore, the measured count rate can be expressed as

$$I = \frac{dI}{d\Omega}\Omega = \frac{dI}{d\Omega}\frac{S}{r^2} = \frac{dI}{d\Omega}\frac{\pi(a^2+h^2)}{(d+h)^2}. \tag{3}$$

S represents the spherical surface onto which the photons are emitted. The quantities r, a, h, and d are illustrated in Figure 1.

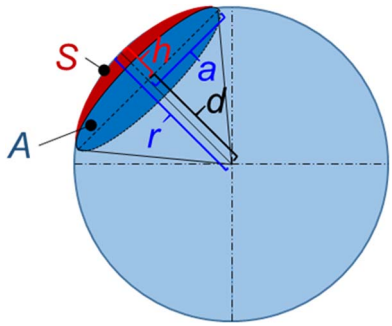

Figure 1. Definition of quantities used in equation (3).

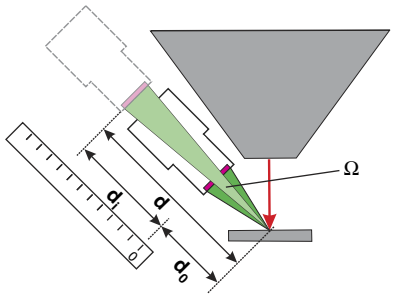

Figure 2. Scheme to measure the detector-specimen distance d. Note that d_0 can be associated to any arbitrary detector position as a reference point.

The detector area, A, corresponds to the base area of S. In order to get A, we apply the approximation

$$I = \frac{dI}{d\Omega}\frac{S}{r^2} \approx \frac{dI}{d\Omega}\frac{A}{d^2}. \tag{4}$$

The approximation in equation (4) has been discussed in two recent papers (Zaluzec, 2009*a*, 2009*b*) and is valid as long as the solid angle does not exceed 1 sr. This approximation is justified for most SEM/EDS configurations, where the solid angle is smaller than 0.1 sr.

The first step of our proposed two-step method to find the effective detector area of an SDD or Si(Li) mounted to the SEM consists in determination of the detector-specimen distance d. Note that d means the distance between the source point on specimen and the detector chip, which is several millimeters behind the front end of the electron trap. d can be found in a simple way when the detector is stepwise retracted and the intensity of an X-ray line at known probe current and live time is measured for the different positions. This is illustrated in Figure 2.

The detector-specimen distance d can always be written as

$$d = d_0 + d_i. \tag{5}$$

d_i is the distance of the detector sensor surface between an arbitrary point on the line between the detector and specimen (e.g., shown by a ruler on the slider for detector

retraction), and d_0 is the distance from that fixed point to the specimen. Inserting equation (5) in equation (4) we have

$$\frac{1}{\sqrt{I}} = \frac{1}{\sqrt{AdI/d\Omega}}(d_0 + d_i). \quad (6)$$

A plot of the reciprocal square root of the count rate versus the EDS detector slide position d_i gives a straight line, having its intersection with the abscissa at $-d_0$. An example is given in Figure 3a for a nominal 80 mm^2 detector. In this case, the slide of the detector had no scale. The abscissa in Figure 3a is the measured distance from the detector flange at the microscope chamber (the fixed point in this case) to the detector housing. This example demonstrates that it is sufficient to measure the relative detector movement only.

Recently, Zaluzec (2009*a*) proposed another method to determine the detector-specimen distance by means of retraction of the detector. Equation (6) can also be written as

$$\ln(I) = \ln\left(A\frac{dI}{d\Omega}\right) - 2\ln(d_0 + d_i). \quad (7)$$

Values for d_0 must be modified in an iterative way until the plot $\ln(I)$ versus $\ln(d_0 + d_i)$ gives a straight line with the slope −2. We applied this method for the example shown in Figure 3a and obtained the straight line with the slope −2 exactly for the same $d_0 = -12.46$ mm, see Figure 3b.

The second step of the method is calculation of the effective detector area A. Inserting equations (1) and (4) in equation (2) we have

$$I = \Omega\epsilon\frac{i_p}{e}\frac{N(\theta)}{4\pi} \cong \frac{A}{d^2}\epsilon i_p f(\chi) Y. \quad (8)$$

$N/(4\pi e)$ was replaced by the X-ray generation yield Y in photons/sr/C. From equation (8) the effective detector area A (mm^2)

$$A = \frac{Id^2}{\epsilon i_p f(\chi) Y}, \quad (9)$$

can be calculated from

(a) measured count rate I (cps), distance d (mm), and beam current i_p (nA),
(b) X-ray yield data Y (photons/C/sr) published as results of measurements with calibrated spectrometers or from fundamental parameter calculations,
(c) calculated absorption correction factors f, which are close to one when K-lines are measured for overvoltage ratios of about 2, and
(d) the detector efficiency ε (counts/photon). For X-ray lines in the range from 2 to 8 keV, ε is practically equal to the transmission of the detector window. Data can be found in the related data sheets (Amptek, 2016; Moxtek, 2016).

Experimental yield data were published for a few selected elements (Green & Cosslett, 1968; Lifshin et al., 1980; Joy, 1998; Procop, 2004). Values are given for K and n in the equation

$$Y = K(U-1)^n, \quad (10)$$

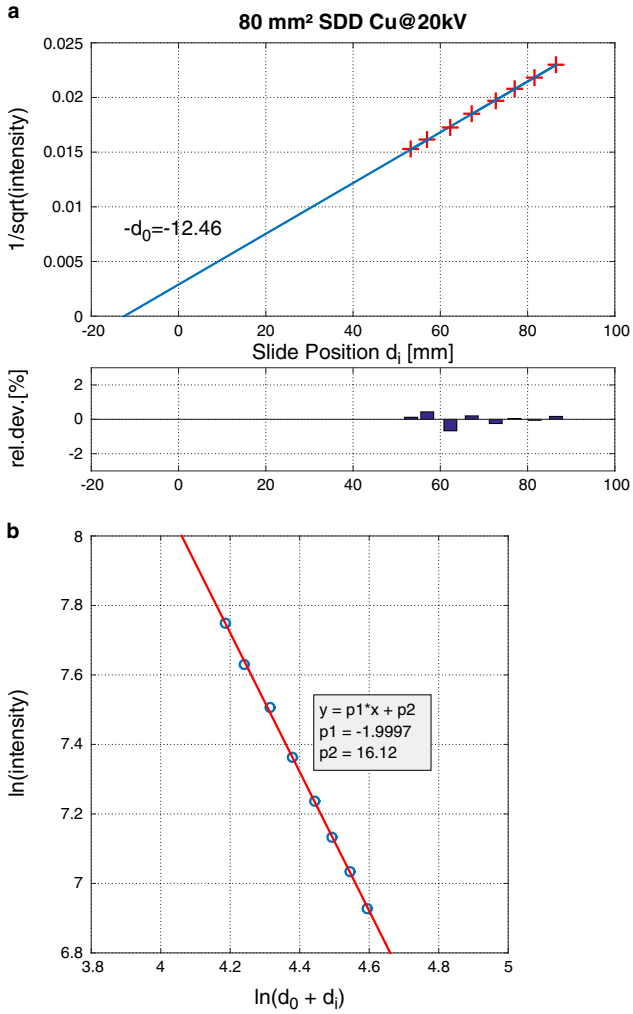

Figure 3. a: Example for a plot according to equation (6). With the detector at working position (at slide position d_i = 50.3 mm), the true specimen-detector distance d amounts to 62.8 mm. **b:** Plot of Zaluzec's method (2009*a*) proposed to determine the detector-specimen distance applied to the same measurement data set as in Figure 3a. The straight line in log–log representation with the slope −2 results in the same d_0 = 12.46 mm. SDD, silicon drift detector.

describing the dependence of the X-ray yield on the overvoltage ratio U. Results for K-lines of copper, titanium, and silicon are compiled in Table 1 and are candidates for determination of the detector area. The table also contains the results of fundamental parameter calculations based on PROZA96 model (Bastin et al., 1998), but modified by the ionization cross-sections (CS) of Casnati et al. (1982); Bote et al. (2009 & 2011), and Powell et al. (2016).

As can be seen in Table 1, there exists some scattering of experimental data. Most results were published for Cu-Kα. For the calculation of detector areas, which will be reported in the next section, yield data from Procop (2004) were used. They were determined with a calibrated spectrometer (Scholze & Procop, 2001). The measurement uncertainty was given as ±5%.

Comparison of experimental and theoretical yield data shows good agreement for silicon (except Joy's result), but

Table 1. Experimental and Theoretical Yield Data in Photons/nC/msr.

Elements and Lines	Procop (2004)	Joy (1998)	Lifshin 1980	Green & Cosslett (1968)	Theory for Casnati CS 1982	Theory for Bote CS 2009	Theory for Powell CS 2016
Cu-Kα at 20 kV	612	567	640	559	663	571	583
Ti-Kα at 10 kV	317	–	293	–	324	297	286
Si-K at 5 kV	379	758	343	–	368	369	356

CS, cross-section.

agreement worsens with increasing atomic number. This is mainly caused by the ionization CS as revealed by related calculations. The new theoretical CS (Bote et al., 2009 & 2011; Powell et al., 2016) were tested, but best results could be achieved with CS calculated with Casnati's empirical formula (Casnati et al., 1982). Absorption and fluorescence corrections are small for the high voltages used, so that the selected matrix correction model should not influence the result.

Results

Evaluation of the Method

First measurements were performed for three spectrometers having a 10 mm^2 SDD, a 10 mm^2 Si(Li), and a 30 mm^2 SDD, respectively. For these three detectors, the size of the aperture in front of the detector chip and hence the net active sensor area was known. The window type was also known. In this way, the achievable accuracy of the method could be evaluated. High voltages for the measurements were selected to have an overvoltage ratio of about 2 for the K-lines of Cu, Ti, and Si, i.e. 20 kV for Cu, 10 kV for Ti, and 5 kV for Si. Under these conditions, the absorption correction factor $f(\chi)$ in equation (1) is close to 1. Beam currents were measured with a calibrated amperemeter (Keithley programmable electrometer 617; Keithley Instruments, Cleveland, OH, USA). Measurements were performed for Cu (pure copper CRM BAM-370), Ti (pure bulk material), and Si (111) wafer. Specimens were positioned at the analytical working distance of the corresponding microscope. The uncertainty in the determination of d_0 by adjusting specimens into the correct working distance can be estimated to be about ±1% as variations of d_0 for three different specimens in Figure 4 show. This number representing statistical precision results from counting statistics, working distance alignment, and reading of d_i. We recommend net peak areas of at least 10,000 counts, so that the corresponding uncertainty stays below ±1%. The determined effective areas and the aperture sizes, which define the "net active sensor area" (cf. ISO 15632, 2012) for these detectors, are compiled in Table 2. Comparison shows that under optimum conditions a total uncertainty level of 5% can be achieved.

Application of the Method to EDS Detectors with Different Areas

Within the frame of this work, the effective area of detectors located in seven laboratories was determined. The results for the 20 kV Cu measurements are compiled in Table 3. Cu has the advantage of lowest uncertainty in spectrometer efficiency ε as well as published X-ray yields Y as mentioned before. For four detectors the effective area is only about the half of the nominal detector area. This was especially surprising for the two 10 mm^2 SDDs in laboratory #5. Indeed, the measured diameter of the collimator cap orifice corresponded with the determined effective detector area.

Comparison with the Aperture Method

For the two detectors in laboratory #1 the effective area was also determined by the aperture method for comparison. This method gives the solid angle of detection from known sizes of apertures placed on the front of the detector's electron trap and the distance between the specimen and apertures. Note that the experiment should be carried out with the EDS detector retracted to the most distant position (e.g., about 10 cm as in the following example). Hence, errors in measurement of the distance to specimen are kept to a minimum, but also possible shadowing effects caused by the support ribs become negligible. Reduction of the illuminated area at large retraction by the opening in the electron trap (an effect that is discussed later in detail) must also be excluded. The geometrical arrangement is sketched in the upper part of Figure 5. The lower part gives the results for this 100 mm^2 detector. The distance between specimen and apertures measured with a ruler amounted to 98 mm. The intensity measured without aperture corresponds to an opening area of 57.2 mm^2 at the position of the apertures. The distance between specimen and detector was determined according to the procedure described above to be 119 mm. To get the effective area on the detector crystal we multiplied the 57.2 mm^2 with the square of the distance ratio of specimen-detector and specimen-aperture. The resulting effective area is 84.1 mm^2.

$$A = 57.2\,\mathrm{mm}^2 \left(\frac{119\,\mathrm{mm}}{98\,\mathrm{mm}}\right)^2 = 84.1\,\mathrm{mm}^2.$$

According to the same procedure, for the 10 mm^2 detector an effective area of 8.5 mm^2 was determined. Both results are inserted in Table 3. The result for the 10 mm^2 detector is close to the known size of the aperture in front of the detector crystal (see Table 2).

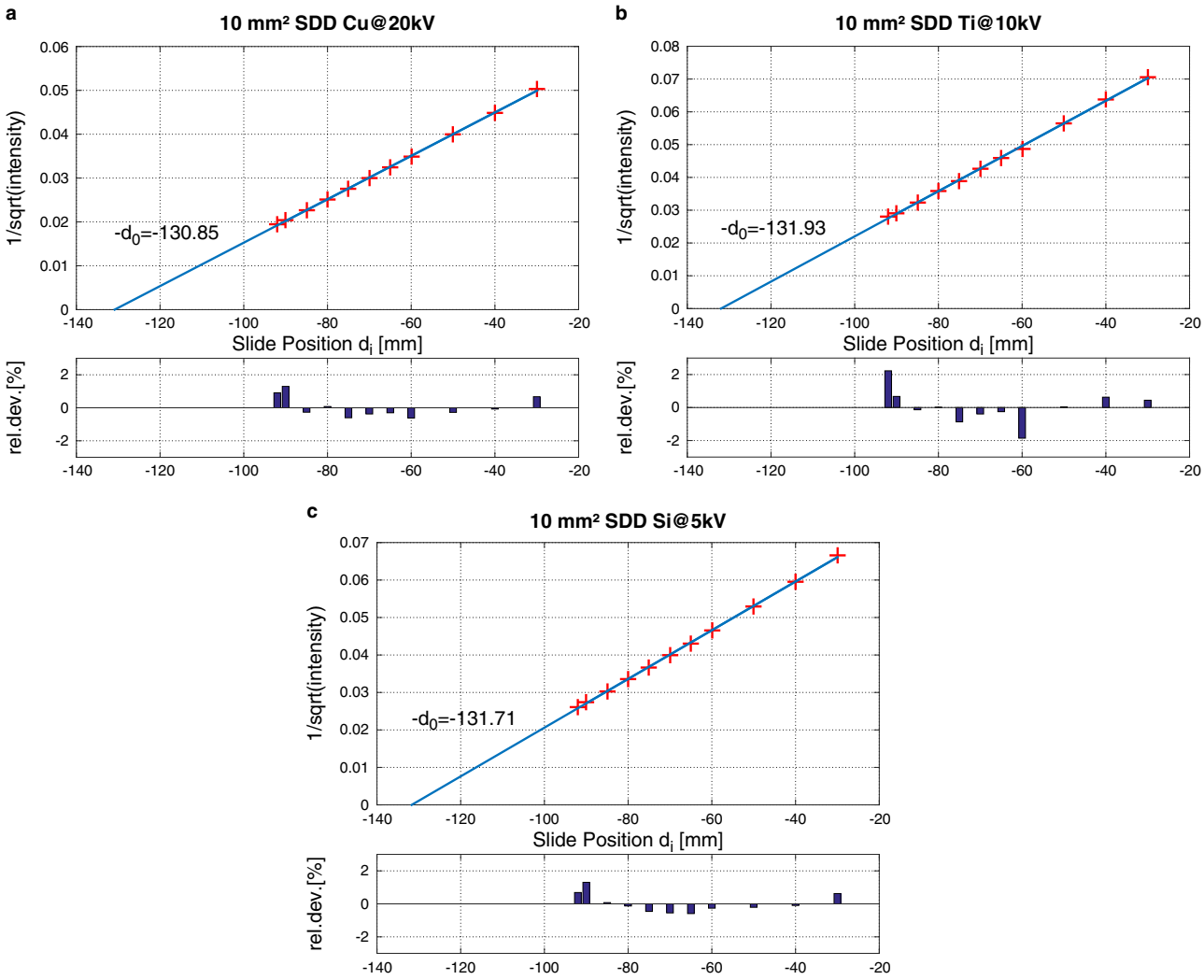

Figure 4. Determination of d_0 for a 10 mm^2 silicon drift detector (SDD) with (**a**) copper, (**b**) titanium, and (**c**) silicon.

Discussion

The results of effective detector area in Table 3 demonstrate that in most cases this area is smaller than the nominal area given by the EDS manufacturer. In cases where the net active sensor area is available from the chip manufacturer, it does not necessarily have to coincide with the effective areas as found by our procedure. Additional to the collimation realized by the chip manufacturer, there may be collimations introduced by the EDS manufacturers when assembling their EDS detectors. For most SEM/EDS detectors, the user knows neither the chip manufacturer, nor the type of collimator and/or electron trap finally installed on a detector.

For many laboratories the low level of 5% uncertainty, which we obtained for the three detectors with known aperture size, will be difficult to achieve. Several factors influence the total uncertainty. An inevitable contribution comes from X-ray yield. It could be reduced by new, dedicated measurements with modern EDS. Most previous measurements were performed with commercial 10 mm^2 Si(Li) EDS systems. More accurate X-ray yields should be expected when measured with a large area SDD in long distance to the specimen to reduce the measurement error for this distance, but not losing the high count rates. Beside X-ray yield, experimental factors contribute to the uncertainty. The first is, perhaps unexpected, beam current measurement. A calibrated amperemeter is usually not available in every laboratory. Moreover, to connect the amperemeter with the SEM, a special cable is required. High-end SEMs have an inbuilt amperemeter. We checked the accuracy of these amperemeters for the four SEMs in laboratories #4 and #5. The deviations to the calibrated instrument were about 2%. This check could not be carried out in laboratories #6 and #7. Unfortunately, some SEMs have no possibility to measure the current. The operator can select a probe current as "spot size," without knowing the true current in nA. When the spectrometer is mounted to such a microscope, the proposed procedure cannot be applied. Beam current measurement is indispensable. It is recommended to check the measurement of beam current by using a calibrated amperemeter.

Calculation of the detector area A according to equation (9) requires knowledge of the spectrometer efficiency ε.

Table 2. Results for the Effective Area of Detectors and Known Aperture Sizes.

Detectors	Elements/Line	Determined A (mm^2)	Known A (mm^2)
SDD 10 mm^2	Cu-Kα at 20 kV	8.8	8.55
	Ti-Kα at 10 kV	8.7	
	Si-K at 5 kV	8.5	
Si(Li) 10 mm^2	Cu-Kα at 20 kV	10.1	9.6
	Ti-Kα at 10 kV	–	
	Si-K at 5 kV	9.2	
SDD 30 mm^2	Cu-Kα at 20 kV	24.1	23.3
	Ti-Kα at 10 kV	22.7	
	Si-K at 5 kV	23.4	

SDD, silicon drift detector.

Table 3. Results for Effective Detector Areas Determined from Measurements with Cu at 20 kV.

Detectors	Laboratory	Area by Yield (mm^2)	Area by App. M. (mm^2)
SDD 10 mm^2	#1	8.8	8.5
Si(Li) 10 mm^2	#2	10.1	–
SDD 10 mm^2	#5	5.3	–
SDD 10 mm^2	#5	6.4	–
SDD 30 mm^2	#3	24.1	–
SDD 30 mm^2	#4	13.7	–
SDD 60 mm^2	#6	65.1	–
SDD 80 mm^2	#4	39.7	–
SDD 100 mm^2	#1	87.2	84.1
SDD 150 mm^2	#7	116.5	–

SDD, silicon drift detector; App. M., aperture method.

It contributes also to the total uncertainty. Results in Table 3 are for the 20 kV spectra of copper. We preferred copper, because ε for Cu-Kα is given only by the transmission of the window. Absorption of X-rays in the front contact of the detector crystal can be neglected in this case. Data for the window transmission can be found in the data sheets of window manufacturers, but uncertainties associated to these data are not given. The transmission in the data sheet gives the grid opening of the window support. These values decrease in case of large area detectors and small distances to specimen due to the oblique incidence of X-rays at the detector periphery. Statham (2010) estimated this effect for a 50 mm^2 SDD positioned at 33 mm to amount to 5% less transmission than at 81 mm for energies below 10 keV. This loss of 5% in intensity propagates into d_0 as square root [see equation (6)], i.e. resulting in about 2.2% error in d_0. Larger detectors cannot be practically inserted to such small distances close to the sample, so that errors significantly higher than 2% can be excluded.

In equation (4), the approximation was made to replace the area of the sphere cap S and its radius r by the bottom area of the cut A and its distance d to the middle point

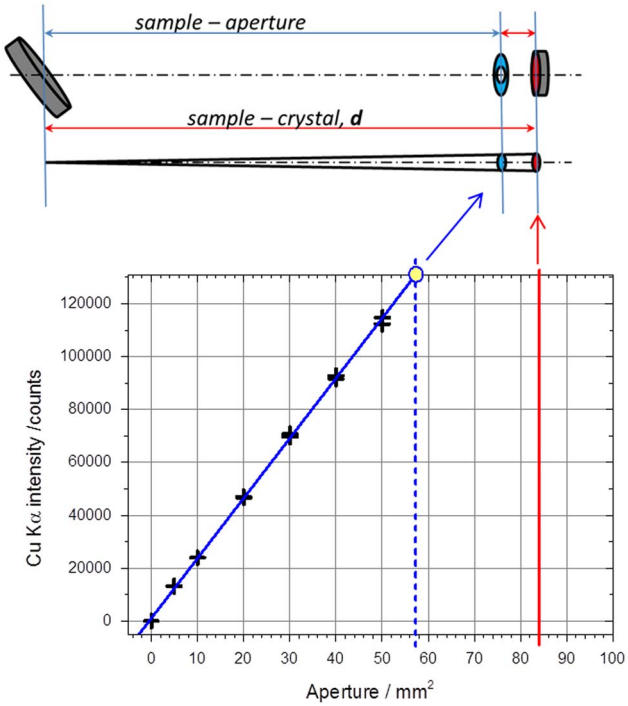

Figure 5. Determination of the effective area of a 100 mm^2 silicon drift detector by means of the aperture method using six different apertures.

(see Fig. 1 for notations). Zaluzec (2009*a*, 2009*b*) discussed this approximation, which might be critical for large area detectors at short distances from the specimen. In principle, the procedure does not depend on the approximation. Without this, A and d in equations (6)–(9) must be replaced by the area of the sphere cap S and the radius of the sphere r. The area A follows from

$$A = S\left(1 - \frac{S}{4\pi r^2}\right).$$

Let us calculate the difference between S and A for the 100 mm^2 detector in Table 3 with the results shown in Figures 7 and 8. The area of the sphere cap S is about 80 mm^2. At a distance of 50 mm, which is in fact the radius r of the sphere, and where the spectrum is already corrupted, the solid angle is only 0.03 sr and the height h of the sphere cap is 0.25 mm. The correct value for the detector area A is then 79.8 mm^2. This means that even in this extreme case of a large area detector close to the specimen, the solid angle remains much smaller than the critical 1 sr and the difference between S and A can be neglected.

A further source of uncertainty is the alignment of the detector. The procedure presumes that the origin of the vector describing the detector motion coincides with the point where the electron beam hits the specimen surface. If this is not the case, 1/sqrt(intensity) versus detector position will not be an exact straight line due to changing take-off angle. Deviations from linearity will be smaller as the

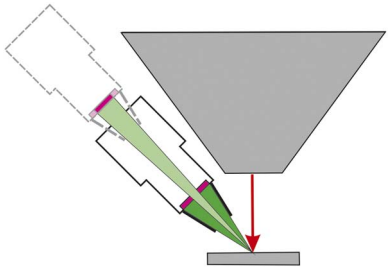

Figure 6. Collimator cap diminishes the effective area when detector is retracted.

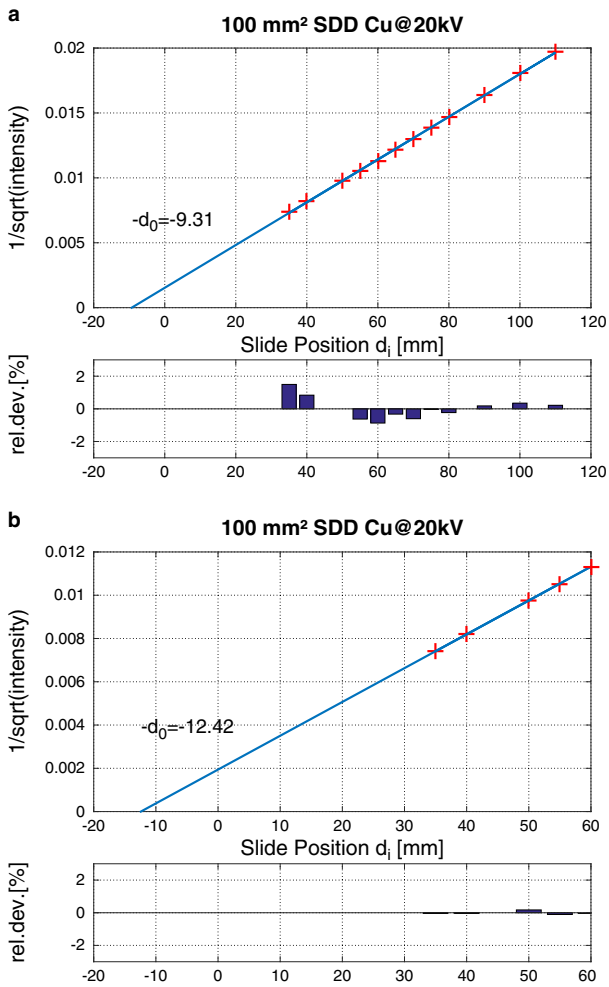

Figure 7. a: All data points, resulting effective area 78 mm^2, (**b**) Only nearest points, resulting area 87 mm^2.

distance is larger. Therefore, from our experience with detectors of known apertures (see Fig. 4), we started our experiments at large distances. For large distances, however, the collimator cap can shadow part of the detector area. This situation is sketched in Figure 6.

An example for such behavior is illustrated in Figure 7 for a 100 mm^2 SDD. Data points in Figure 7a seem to be on a straight line intersecting the abscissa at −9.31 mm. The calculated effective area is 78 mm^2. But a plot of the relative

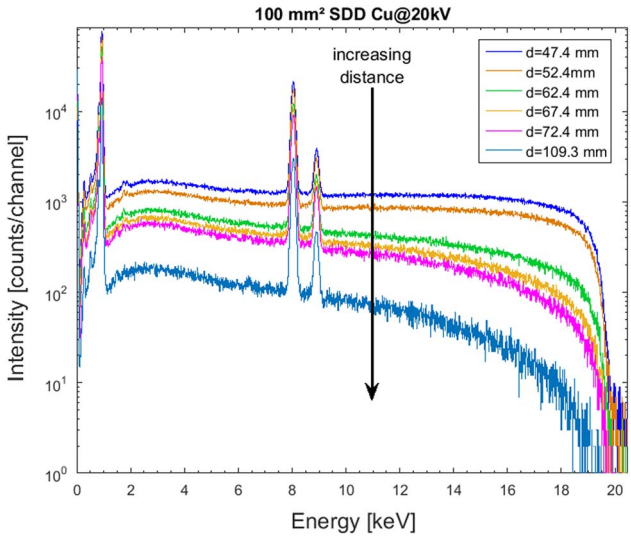

Figure 8. Cu spectra for the data points in Figure 7. SDD, silicon drift detector.

deviations from the straight line reveals a systematic tendency. Fitting only the five points with shortest distances by a straight line results in the intersection of the abscissa at −12.5 mm (see Fig. 7b). The resulting effective area increases to 87 mm^2. However, for such small specimen-detector distances this particular collimator cap appears to lose its efficiency to deflect backscattered electrons. It should be noted here that these short distances are smaller than the distance suggested by the service at installation. The corresponding X-ray spectra show an increased background at high energies, which cannot be described by Kramers law (see Fig. 8). Only at specimen-detector distances above 70 mm is an acceptable spectrum measured. At these distances, the corresponding effective area is 78 mm^2.

Concerning optimum experimental conditions a conflicting situation exists. At large specimen-detector distances, the influences of X-ray beam divergence, alignment uncertainties (working distance and take-off angle), and the relative error in d_i metering are minimized. On the other hand, retraction of the detector may result in a shadowing of the detector area by the electron trap, which might not necessarily occur at the designated detector position close to the specimen. An example of such a situation is demonstrated in Figure 7. It is recommended, therefore, to start at the detector working position closest to the specimen with small d_i in steps of 1–3 mm and to observe carefully any deviation from a fitted straight line which might occur after about 1 cm retraction. Deviations should be of statistical nature only as in Figure 3a, caused by counting statistics and d_i uncertainty only.

Considering all potential sources of uncertainty associated to the effective area as determined by the proposed procedure, i.e. about 5% for X-ray yield, about 2% in d_0^2 and further minor contributions from beam current measurement and window transmission, the total measurement uncertainty of the resulting effective area of 10% is attainable by a carefully performed experiment in every laboratory.

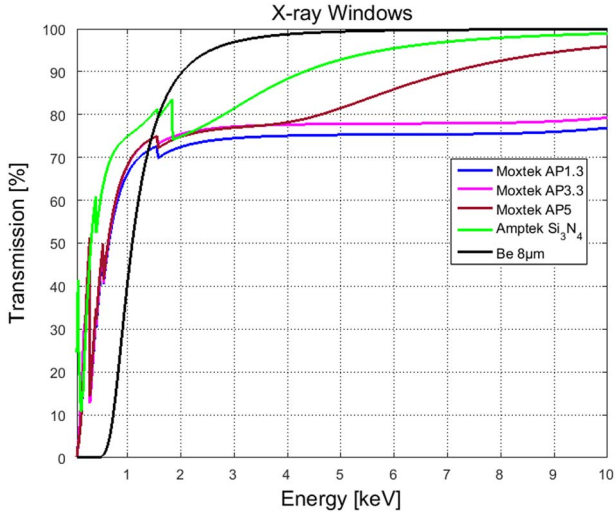

Figure 9. X-ray transmission for different detector window types.

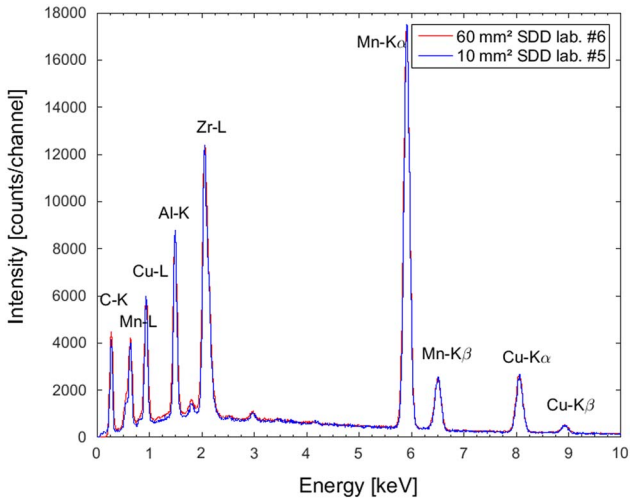

Figure 10. 20 kV EDS-TM002 spectra measured with 60 mm^2 silicon drift detector (SDD) in laboratory #6 and 10 mm^2 SDD in laboratory #5, both equipped with Moxtek AP3.3 window.

In the last 20 years, the majority of EDS for SEMs was equipped with thin film windows AP1.3 and later AP3.3 from the Moxtek company (MOXTEK, Inc., Orem, UT, USA). Their transmission is given in the related data sheets and amounts to 77% at Cu-Kα. Recently, new window types were developed with higher transmission for Cu-Kα. Looking at the transmission of the four types of thin film windows in Figure 9, effective area determination using the X-ray yield for a line at 2 keV could be a better approach because transmissions are similar. Intensive lines at this energy are Zr-Lα (2.04 keV), Pt-Mα (2.05 keV), and Au-Mα (2.12 keV). Joy (1998) published yield data for the Mα lines of Pt and Au.

As long as reliable yield data in the 2 keV range are not yet available, BAM test material EDS-TM002 (Hodoroaba & Procop, 2014; BAM Webshop 2016) opens an alternative way to find the window type in case it is not known. The test material was developed to determine the efficiency of X-ray spectrometers (Alvisi et al., 2006). EDS-TM002 is a 6 μm thick film consisting of carbon, aluminum, zirconium, manganese, and copper on silicon substrate. The deposition method ensures a homogeneous composition for all specimens. Line intensity ratios are very sensitive against changes of window transmission. We applied EDS-TM002 to identify the window type of the 60 mm^2 detector in laboratory #6 listed in Table 3. This detector is the only one in the table, for which the effective area determined by our procedure exceeds the nominal area. It was a new detector; a window with a transmission above 90% at Cu-Kα could not be excluded *a priori*. In the case of a new window type, the resulting effective area would be <60 mm^2. In order to get the necessary information concerning window transmission, we compared the 20 kV spectra of EDS-TM002 measured with this detector with the spectrum measured with the 10 mm^2 SDD having an AP3.3 window in laboratory #5. Both have the same manufacturer. Spectra match completely (see Fig. 10) indicating that the 60 mm^2 SDD was also equipped with the AP3.3 window. However, next-generation detectors will be equipped with the new polymer, Si_3N_4 and perhaps graphene (Huebner et al., 2015) windows. The test material EDS-TM002 can be applied to identify next-generation windows by comparing line intensity ratios. Table 4 gives relative line intensity ratios in the spectra of EDS-TM002 for the window types in Figure 9. Ratios for Moxtek AP5 and Amptek Si_3N_4 were calculated from the transmission curves in Figure 9 and measured intensities for a detector equipped with a Moxtek AP3.3 window.

Table 4. Relative Line Intensity Ratios in 20 kV spectra of EDS-TM002 at take-off angle = 35°.

	Intensity Ratios	
Window Type	Mn-Kα/Zr-L	Cu-Kα/Zr-L
Moxtek AP3.3	1.44	0.23
Moxtek AP5	1.59	0.27
Amptek Si_3N_4	1.78	0.28

Conclusions

A procedure for determination of the effective area of an EDS detector is proposed. It consists in principle of measurements of K line intensities, e.g. of pure copper at 20 kV, and their comparison with calculated intensities using known X-ray yield data from the literature. The solid angle, necessary for the calculation, is determined from measurements at different detector-specimen distances. The procedure gives an SEM/EDS operator the opportunity to determine the effective detector area within an uncertainty range of ±10%. The main uncertainty sources are X-ray yield, beam current measurement, window transmission and positioning the specimen at the correct working distance. Preconditions to

apply the procedure are accurate probe current measurement and the possibility to retract the detector without introducing any occlusion of the detector area.

Knowing the detector window type and its transmission is necessary to calculate the X-ray intensities. For cases where the type of detector window is unknown to the user, which might be expected due to the current rapid development of new window types, we propose (1) to measure either an X-ray line at about 2 keV with known X-ray yield or (2) to identify the window type from measured 20 kV spectra of the commercial test material EDS-TM002 and apply the procedure with the copper X-ray yield at 20 keV as in this paper.

Results for ten different detectors show that in most cases the effective detector area is smaller than the nominal detector area given (and not specified) by the manufacturer. One of the reasons is an aperture in front of the detector chip to prevent illumination of the border area. Significant smaller effective areas (50% and more) for the 10 and 30 mm^2 detectors are probably caused by the opening in the electron trap which is too small for the specific specimen-detector distance recommended at installation. It should be emphasized that the effective area determined by the proposed procedure relates to a specific installation of an EDS to the SEM. It is not a quantity, which specifies the EDS. However, in the ideal case of no additional shadowing of the detector, the determined effective area is in agreement with the net active sensor area that should be specified by the EDS manufacturer according to ISO 15632 (see examples in Table 2).

Acknowledgments

The authors thank Dr. W. Österle, Dr. G. Nolze and N. Wollschläger (all from BAM-5.1); Dr. P.-F. Schmidt (Akademie für Elektronenmikroskopie und Analytik gGmbH, Münster, Germany); and Dr. M. Schleifer (AMETEK GmbH, EDAX Business Unit, Wiesbaden, Germany) who have helped the authors to take measurements in their respective laboratories.

References

Alvisi, M., Blome, M., Griepentrog, M., Hodoroaba, V.-D., Karduck, P., Mostert, M., Nacucchi, M., Procop, M., Rohde, M., Scholze, F., Statham, P., Terborg, R. & Thiot, J.-F. (2006). The determination of the efficiency of energy dispersive X-ray spectrometers by a new reference material. *Microsc Microanal* **12**, 406–415.

Amptek (2016). C-series low energy X-ray windows. Available at http://amptek.com/product/c-series-low-energy-x-ray-windows (retrieved October 5, 2016).

Bam Webshop (2016). Reference materials, test materials Available at www.webshop.bam.de/ (retrieved October 5, 2016).

Bastin, G.F., Dijkstra, J.M. & Heijligers, H.J.M. (1998). PROZA96: An improved matrix correction program for electron probe microanalysis, based on a double Gaussian φ(ρz) approach. *X-Ray Spectrom* **27**, 3–10.

Bote, D., Salvat, F., Jablonski, A. & Powell, C.J. (2009 & 2011). Cross sections for ionization of K, L and M shells of atoms by impact of electrons and positrons with energies up to 1 GeV: Analytical formulas. *At Data and Nucl Data Tables* **96**, 871–909. & Erratum. ibid. 97, 186.

Casnati, E., Tartari, A. & Baraldi, C. (1982). An empirical approach to K-shell ionisation cross section by electrons. *J Phys B: At Mol Phys* **15**, 155–167.

Castaing, R. & Descamps, J. (1955). Sur les bases physiques de l'analyse ponctuelle par spectrographie X. *J Phys Radium* **16**, 304–317.

Green, M. & Cosslett, V.E. (1968). Measurements of K, L and M shell X-ray production efficiencies. *Br J Appl Phys (J Phys D) Ser 2*, **1**, 425–436.

Hodoroaba, V.-D. & Procop, M. (2014). A Method to test the performance of an energy-dispersive X-ray spectrometer (EDS). *Microsc Microanal* **20**, 1556–1564.

Huebner, S., Miyakawa, N., Pahlke, A. & Kreupl, F. (2015). Design and properties of low-energy X-ray transmission windows based on graphenic carbon. *Phys Status Solidi B* **252**(11), 2564–2573.

Kemmer, J., Lutz, G., Belau, E., Prechtel, U. & Welser, W. (1987). Low capacity drift diode. *Nucl Instrum Methods Phys Res A* **253**, 378–381.

Ketek (2016). VITUS SDD. Available at http://www.ketek.net (retrieved October 5, 2016).

ISO 15632 (2012). *Microbeam Analysis—Selected Instrumental Performance Parameters for the Specification and Checking of Energy-Dispersive X-Ray Spectrometers for Use in Electron Probe Microanalysis*. Geneva: ISO.

Joy, D.C. (1998). The efficiency of X-ray production at low energies. *J Microsc* **191**(Pt 1), 74–82.

Lifshin, E., Ciccarelli, M.F. & Bolon, R. (1980). Ch. III. Energy dispersive spectrometry. In *Proceedings of 8th ICXOM, Boston 1977*. Beaman, D.R., Ogilvie, R.E. and Wittry, D.B. (Eds.), pp 141–148, Midland, MI: Pendell.

Maenhaut, W. & Raemdonck, H. (1984). Accurate calibration of a Si(Li) detector for PIXE analysis. *Nucl Instrum Methods B* **1**, 123–136.

Moxtek (2016). AP X-Ray windows. Available at http://moxtek.com/xray-product/ap-windows/ (retrieved October 5, 2016).

Oxford Instruments (2016). Available at https://www.oxford-instruments.com/ (retrieved October 5, 2016).

Powell, C.J., Llovet, X. & Salvat, F. (2016). Use of the Bethe equation for inner-shell ionization by electron impact. *J Appl Phys* **119**, 184904. (17pp.).

Procop, M. (2004). Measurement of X-ray emission efficiency for K-lines. *Microsc Microanal* **10**, 481–490.

Procop, M., Hübner, W., Wäsche, R., Nieland, S. & Ehrmann, O. (2002). Fast elemental mapping in materials science. *Microsc Anal* (January), 17–18.

Scholze, F. & Procop, M. (2001). Measurement of detection efficiency and response functions for an Si(Li) X-ray spectrometer in the range 0.1-5 keV. *X-Ray Spectrom* **30**, 69–76.

Statham, P.J. (2010). Improved efficiency characterisation for large solid angle SDD detectors. *Microsc Microanal* **16**(Suppl 2), 1304–1305.

Zaluzec, N.J. (2009*a*). Detector solid angle formulas for use in X-ray energy dispersive spectrometry. *Microsc Microanal* **15**, 93–98.

Zaluzec, N.J. (2009*b*). Calculating the detector solid angle in X-ray energy dispersive spectroscopy. *Microsc Microanal* **15**(Suppl 2), 520–521.

Zaluzec, N.J. (2014). Analytical formulae for calculation of X-ray detector solid angles in the scanning and scanning/transmission analytical microscope. *Microsc Microanal* **20**, 1318–1326.